Contract No.:

This manuscript has been authored by Battelle Savannah River Alliance (BSRA), LLC under Contract No. 89303321CEM000080 with the U.S. Department of Energy (DOE) Office of Environmental Management (EM).

SRNL-STI-2021-00543, Rev. 1

Modeling Gas Release from a Bingham Plastic Slurry and Deconvoluting Measured Data

Michael R. Poirier[1,*], John A. Thomas[2] and John Pareizs [1]

1) Savannah River National Laboratory Aiken, SC 29808, USA
2) M-Star CFD, 11100 Baltimore National Pike Ellicott City, MD 21042, USA

Keywords

Two-phase fluid, off-gassing, agitated tank, CFD, yield stress fluid

Abstract

Physics-based models for predicting the off-gassing characteristics of agitated slurries are presented. This approach decomposes the system into two separate but coupled slurry and headspace models. The physics driving bubble transport through the slurry and gas mixing within the headspace are discussed. An analytical expression for predicting the time evolution of the headspace concentration using first principles theory is also presented. Predictions from the numerical models, as well as expectations from the analytical solution, both agree with measured off gassing data for two different experimental operating conditions. After benchmarking the numerical model predictions against experimental data, the model was used to make predictions for gas release from a full-scale vessel and to perform sensitivity analyses to examine the sensitivity of gas release to parameters such as yield stress, consistency index, slurry density, bubble size, bubble concentration, and impeller speed.

1.0 Introduction and Motivation

Slurry off-gassing, which involves the controlled release of gas bubbles trapped inside a viscous fluid, is a key unit operation in defense waste treatment and clean-up processes. (1) Such operations typically use mechanical agitation to advect bubbles from the interior of the slurry to the free surface, where the bubbles burst to release their trapped gas into the tank headspace. Because these trapped gasses may be flammable and/or toxic, the headspace environment above the slurry must be continuously purged to prevent a hazardous build-up of off-gassed materials. A well-designed process is one that provides control over gas release from the slurry while simultaneously keeping the headspace environment within acceptable safety limits.

The slurries relevant to defense/radioactive waste treatment are typically radioactive and generate hydrogen that must be released in a controlled fashion. (2) These properties, which require small sample volumes and non-contact testing, make measurement and experimental characterization difficult. Numerical models, built using first-principles transport relationships, can provide an effective tool to designing off-gassing unit operations involving such materials and for understanding how slurry properties and process operating parameters affect the off-gassing. Beyond providing guidance on process outcomes, these models can also (i) elucidate the underlying physics driving system behavior and (ii) assess the impact of slurry properties and operating conditions on the off-gassing process. Moreover, for previously measured headspace concentration data, these numerical models can help deconvolute the competing effects of the mixing in the headspace from the off-gassing properties of the slurry.

Much of the previous work investigating the release of gas bubbles from viscous/non-Newtonian fluids has been in unagitated tanks, and it has focused on comparing viscous forces and buoyancy forces and determining the critical yield stress at which bubble rise would cease. (3) (4) Johnson et al., used lattice-Boltzmann modeling and Monte Carlo simulations to investigate the permeability of gas bubbles in cohesive sediments. (1) Gauglitz et al. and Rassat et al. investigated retention and release of entrained gases in underground storage tanks and determined that the yield stress and particle size have the most significant effect on the retention and release of flammable gases. (5) (6)

Within the context of agitated systems, Russell et al. performed a series of hydrogen retention tests in tanks mixed using pulsed jet mixers. The tests provided correlations of the rheology, bubble size, and the gas retention and release properties of the fluids. (7) Patel et al. performed gas retention and release experiments with low yield stress kaolin/bentonite slurries agitated by an impeller. When agitation started, the initial gas release showed a peak around 2-3 minutes followed by a steady decay over a period of 100 minutes. (8) Although this system is somewhat like the agitated tanks considered

here, the report did not include any mechanistic analysis of the results. As such, although the overall pattern of an initial burst of off-gas followed by a long/slow release is insightful, the results cannot be generalized to arbitrary agitated systems.

Tangentially, some work has been done in understanding gas release from sparged bioreactors, as related to changes in headspace gas composition. (9) Within such systems, gas bubbles are continuously added to the vessel to modify the concentration of any dissolved gases. If the headspace turnover rate is slow compared to the gas injection rate, the composition of the headspace gases will evolve in time to reflect the composition of the bubbles exiting the fluid. In some applications, quantifying the time-evolution of species within the headspace provides insights into sparging efficiency, cell health and overall process outcomes. (10) Although mechanistically like the off-gassing work considered here, the physics governing this behavior are very different. Compared to high-viscosity slurries, for example, bubbles in bioreactors are moving through turbulent flows. Moreover, compared to the continuous sparging of a bioreactor, the off-gassing process considered here is a longer scale process involving the slow-release of a fixed quantity of gas.

In this work, we attempt to generalize and extend these previous efforts by developing a set of physics-based modeling approaches for predicting the off-gassing properties of Bingham plastic slurries and the associated response of the purged headspace. Although applied here to radiochemical fluids with trapped hydrogen bubbles, the approach can be applied to arbitrary slurry systems with or without ongoing gas generation. The key element of this approach is a decomposition of the system into two distinct but coupled models: (i) a slurry model used to predict bubble release due to agitation and (ii) a headspace model used to predict the off-gas mixing within the purged gas. We compare the predicted to measured off-gas data for two data sets at two different scales. We also compare predictions to an analytical solution, as derived from two well-stirred tanks in series. After benchmarking the models against experimental data, the models can be applied to a full-scale vessel to predict off-gassing rates.

We begin in Section 2.0 by summarizing the key physics driving off-gassing and an overview of the measurement process. Next in Section 3.0, we introduce and discuss the conservation laws and governing equations used to build the models. These conservation laws include the Navier-Stokes equations, Newton's Second Law, and the conservation of mass. In Section 4.0, we apply this approach to a 342 mL slurry sample and compare the predicted off-gassing rate against measured data. We also develop an expression for predicting the measured response of the purged headspace gas using known slurry and headspace turnover time. Next, in Section 5.0, we apply this approach to a 1 liter sample of slurry. We compare the predicted cumulative off-gas rate to measured data, as well as expectations from first principles. The agreement at both the 342 L and 1 L systems is good, despite differences in the overall system responses at each scale. In Section 6.0, we apply the model to a full-scale vessel (31.2 m^3) to predict the rate of hydrogen gas bubble release and the maximum hydrogen concentration in the headspace. In addition, in Section 7.0, we perform sensitivity analyses to examine the effect of parameters such as slurry yield stress, slurry consistency index, slurry density, bubble size, bubble concentration, and impeller speed on the gas release rate. We conclude in Section 8.0 with a summary of the work here and future opportunities.

2.0 Process Overview and Modeling Approach

Slurry off-gassing rates are typically characterized using controlled purge processes. Within these processes, as illustrated in Figure 1, a volume of slurry V_s is transferred to a sampling vessel where the headspace volume V_H is continuously renewed by a stream of purge gas. The gas flow into the headspace, which enters at a known flow rate $\dot{V}_{in}$, is well characterized and inert. Moving through the headspace, however, the purge gas mixes with gasses coming off the slurry. If the flow rate of the released gas $\dot{q}_t$ is small relative to $\dot{V}_{in}$, the volume flow rate of purge gas exiting the headspace will be indistinguishable from that entering the headspace. The composition of this exiting headspace gas,

however, will be an evolving mixture of purge gas and slurry off-gas. As such, the measured time-evolution of this exiting gas concentration $q(t)$ will be a convoluted function of $\dot{q}_t$, $\dot{V}_{in}$ and V_H. When using a controlled purge to characterize off-gassing, a decomposition is required to isolate $\dot{q}_t$ (the relevant physical property) from $q(t)$ (the measurable system response).

From the perspective of the slurry, gas transport and off-gassing occur as individual bubbles arrive at the free surface and burst to release its contained gas into the headspace. In most high viscosity slurries, the buoyant force on an individual bubble is insufficient to overcome the yield stress of the fluid. (11) (12) As such, to introduce off-gassing, ongoing agitation is required to fluidize the slurry and advect bubbles from the fluid bulk to the free surface interface. Although the bubble diameter d_b and the bubble density ρ_b inform the volume of gas inside each bubble, the removal rate $\dot{q}_t$ is primarily dependent on the impeller speed N, fluid viscosity μ, and fluid yield stress τ. In principle, radiolysis can lead to ongoing gas bubble formation during the agitation process. In practice, however, the additional gas formed during agitation will be order-of-magnitude smaller than the gas accumulated during storage. As such, for the off-gassing processes considered here, it is appropriate to assume that the gas bubble population decreases monotonically with time due to bursting at the free surface.

From a modeling perspective, both bubble transport within the slurry and gas transfer within the headspace must be described to properly model the purging process. Since the physics in the slurry are largely decoupled from the flow in the headspace, we can decompose this model into two components: (i) a two-phase slurry model and (ii) a single-phase head-space model. The two-phase slurry model is used to model bubble generation and bubble transport within the slurry due to mechanical agitation. The inputs to this model include any gas generation rates, the tank/impeller topology, the system operating conditions, the density/rheology of the slurry and the physical properties of the gas bubbles. Output from this model includes the flow field within the vessel, the rate at which bubbles are leaving the system, and the time (and position)-evolution of the bubble population within the slurry. For

systems without ongoing bubble generation, the bubble population balance will decrease monotonically in time as bubbles continuously exit through the free surface.

The single-phase headspace model is used to model gas transport within headspace and the competition between purge rate and off-gassing rate. The inputs to this model include the purge gas flow rate, the headspace/nozzle topology, the physical properties of the gas, and the time evolution of the off-gassing profile. Note that this final input to the headspace model is the output from the two-phase slurry model. The data generated by the single-phase headspace model includes the spatial variation of the released gas concentration across the headspace, as well as the time-evolution of the gas concentration leaving the headspace. The composition of this exit stream is directly comparable to measured data. This comparison, in tandem with expectations from first principles, and will be used to validate the models.

3.0 Implementation Details

3.1 Fluid Flow

In both the slurry and headspace models, we describe fluid flow using the incompressible Navier-Stokes equations. The Navier-Stokes equations, which model the conservation of momentum of a fluid particle, can be written as:

$$\frac{\partial \vec{V}}{\partial t} + \vec{V} \cdot \nabla \vec{V} = g - \frac{\nabla p}{\rho} + \nabla \cdot \left(\nu \nabla \vec{V}\right), \quad (1)$$

where $\vec{V}$ is the velocity of the fluid particle at a given location at a given time, g is the acceleration due to gravity, p is pressure, ρ is the fluid density, and ν is the fluid kinematic viscosity at a given location and t is time. (13) Note that this expression is inherently transient: the left-hand side represents the acceleration of the fluid particle, while the right-hand side represents the forces due to gravity, pressure gradients, and shear stress. Note that, when solving Equation 1, we assume that the fluid is incompressible:

$$\nabla \cdot \vec{V} = 0, \quad (2)$$

where ∇ is the divergence operator.

We solve the Navier-Stokes using a linearized form of the Boltzmann transport equation. The Boltzmann transport equation, which models the conservation of transport carrier probability density, can be written as: (14)

$$\frac{\partial f}{\partial t} + \vec{v} \cdot \nabla f = \Omega(f, f), \quad (3)$$

where f represents the probability density function, $\vec{v}$ represents the phase space velocity, and Ω represents a collision operator. The Navier-Stokes equations are solved by linking f to the fluid momentum and $\Omega(f, f)$ to the fluid kinematic viscosity. (15) When solving Equation 1, we discretized the velocity space using a D3Q19 lattice and relax the distribution using the Bhatnagar–Gross–Krook (BGK) operator. Fluids interact with the tank walls via a no-slip boundary condition, as enforced via a zero-velocity bounce back method. Fluids interact with the moving impeller and shaft via the immersed boundary method, which enforces a no-slip velocity boundary condition along the impeller/shaft surfaces as they move through the fluid. (16) The top surface of the fluid is modeled as a dynamic free surface using a volume-of-fluid approach. (17)

3.2 Bubble Transport

Within the slurry model, bubbles are tracked individually as discrete spheres assumed to be small relative to the fluid cells. Bubble trajectories are governed by Newton's second law, such that: (18)

$$m_i \vec{a}_i = \vec{F}_{i,g} + \vec{F}_{i,a} + \vec{F}_{i,p} + \vec{F}_{i,D} \quad (4)$$

where m_i and $\vec{a}_i$ represent the mass and acceleration vector of bubble i, $\vec{F}_{i,g}$ is the gravity force, $\vec{F}_{i,a}$ is the added mass force, $\vec{F}_{i,p}$, is the instantaneous pressure gradient force, and $\vec{F}_{i,D}$ is the instantaneous drag force on the bubble. (19) Equation 4 is solved for each bubble individually and in tandem with the fluid algorithm using the velocity Verlet algorithm. (20)

In accordance with Newton's third law, particles are two-way coupled to the fluid, such that a body force at each fluid lattice voxel, $\vec{F}_{f,j}$:

$$\vec{F}_{f,j} = -\sum_i^{i\in j} \vec{F}_{i,a} + \vec{F}_{i,D} \quad (5)$$

is superimposed on the fluid lattice voxel j containing the set of bubbles $i \in j$. Note that this fluid body force does not include the pressure gradient force on the bubble, as this force is already incorporated into Equation 1. Although practical to implement, bubble coalesce, break-up, and mass transfer, were not included in this model.

3.3 Species Transport

In the headspace model, species transport is modeled via the advection-diffusion-reaction equation: (13)

$$\frac{dc_j}{dt} = \nabla \cdot \left(D\nabla c_j\right) - \nabla \cdot \left(\vec{v}_j c_j\right) + \frac{\dot{n}_j}{V_j} + R_j \quad (6)$$

where c_j is the species concentration in fluid lattice voxel j, D is the gas diffusion coefficient, $\vec{V}_j$ is the fluid velocity vector, V_j is the volume of the fluid lattice voxel, $\dot{n}_j$ is the species transfer rate between the bubbles and the fluid in voxel j, and R_j is the local species production rate. We use the lattice-Boltzmann particle velocities to solve Equation 6 at each timestep for each fluid voxel.

3.4 Implementation

The computational models were built and solved using M-Star CFD®, a GPU-based computational physics package tailored to chemical engineering simulations. (21) Compared to traditional finite element and finite difference approaches, the LBM-based approach applied here provides a multiple order-of-magnitude improvement in computational speed when solving Equations 1, 4, and 6. (22) This trend is amplified in graphics processing unit (GPU)-based computing environments, which can fully exploit the localized nature of the Boltzmann transport equation. At present, running LBM on GPU is the most efficient approach to solving the transient Navier-Stokes equations. (23)

All simulations were executed with a uniform grid spacing of 350 lattice points across the vessel diameter and a Courant number of 0.1. This grid spacing has been shown previously to provide fully converged power and blend-time predictions across the range of viscosities relevant to this work. (24) (25) The Courant number, which informs the simulation timestep and fluid compressibility, is sufficient to keep density fluctuations below 1-2%. Simulation runtimes were set to 1000 seconds to 7500 seconds, depending on system scale.

4.0 342 mL System

In Figure 2, we present the slurry model used to study a 342 ml volume sample. The vessel is a cylindrical 11 cm-diameter vessel agitated by a 0.05 m diameter flat blade impeller. The impeller speed is 170 RPM. The free surface level was set to 0.035 m. The slurry was modeled as a Hershel-Buckley (Bingham plastic) fluid with the constitutive relationship:

$$\tau = \tau_o + k\gamma^n \quad (7)$$

where τ_o is the yield stress, k is the consistency index, and n is the flow index. The rheology parameters applied to both the 342 ml and 1 L models, which were determined by previous measurement, are summarized in Table 1.

The gas bubbles were modeled as 13,376 individual monodisperse spheres. All bubbles were added to the slurry uniformly and instantaneously prior to the first simulation timestep. No additional bubbles were generated during agitation. Conceptually speaking, this injection profile implies that the gas generated during agitation is negligible relative to the gas generated during storage. The initial bubble size was set to 310 micrometers, a value consistent with experimental characterization of the slurry, test operating parameters, and the following correlation from Machon et al. (26)

$$d_{32} = 2.25 \frac{\sigma^{0.6}}{(P/V)^{0.4}\rho^{0.2}} \epsilon_H^{0.4} \left[\frac{\mu_G}{\mu_L}\right]^{0.25} \quad [8]$$

where d_{32} is the Sauter mean diameter of the bubble, σ is the surface tension of the bubble, P/V is the applied power per unit volume, ρ is the fluid density, ε_H is the gas hold up fraction, μ_G, is the gas viscosity, and μ_L is the liquid viscosity.

In Figure 3, we present snapshots of the velocity and the bubble fields. The spatial variations on the velocity field reflect the competing effects of inertia and viscosity within the fluid. Near the impeller, per requirements of the no-slip boundary condition, the velocity is equal to the impeller tip speed. At the wall, again per the no-slip boundary conditions, the velocity is zero. The velocity dead-zones in the corners of the vessel reflect the finite yield stress of the fluid. (27) At this impeller speed, the effective cavern diameter is equal to the tank diameter and most of the fluid is in motion. In the corners of the tank, however the shear stress of the flow is insufficient to overcome the yield stress of the fluid. Despite an overall decrease in the total bubble count with time, the bubble distribution remains relatively uniform across the moving portions of the vessel. This trend corroborates the idea that release is governed by bubble advection across the tank. More specifically, if buoyancy were the driving factor informing bubble removal, with increasing time the bottom portion of the tank would become

increasingly bubble-free relative to regions near the middle of the vessel. This result is in line with expectations from the Stokes number.

In Figure 4, we present the time evolution of the bubble flux across the free surface interface. Predictions in the model suggest a peak after about 20 seconds of agitation, followed by a gradual decrease in flux across the free surface. To help characterize this profile, we superimpose on the profile the flux expected for a well-stirred system: (28)

$$\frac{dC_s(t)}{dt} = -(1/\tau_s)C_{s,o}e^{(-t/\tau_s)} \quad (9)$$

where C_s is the gas concentration in the slurry, τ_s is the off-gassing time scale, and t is time. Recognize that the gas concentration is linked to the bubble number density via the ideal gas law, such that:

$$C_s(t) = \frac{N_B V_B V_m}{V_s}, \quad (10)$$

where N_B is the number of bubbles, V_B is the (individual) bubble volume, V_M is the molar volume of the gas, and V_S is the volume of the slurry. The best fit value of τ_s is determined to be 133 seconds. The authors make the assumption that the hydrogen release is contant across the slurry-gas boundary with no radial variation and no circumferential momentum. Because of fluid motion in the slurry, a radial variation in released gas flux may occur. In addition, rotational motion of the slurry may inpart a circumferential velocity to the released gas. Images of the headspace show the fluid motion and concentration profile to be very turbulent. Any non-uniformity in released gas flux that may occur in the radial direction would be corrected by the turbulent mixing that occurs in the headspace.

Deviations between the predicted outgassing rate and expectations from the theoretical model in Equation 9 are indicative of non-ideal ideal mixing patterns within the fluid. In the first 60 seconds of agitation, for example, the fluid is being accelerated by the impeller and converging to a steady state flow field. Accordingly, the predicted outgassing rates oscillate about expectations from Equation 9.

After the start-up period, however, the predicted release rate follows the first principles trend. This fit will be used an input to the headspace model, as well as input to the analytical solution discussed below.

In Figure 5, we present the headspace model used to simulate the headspace purge of the 342 mL sample. The vessel was a cylindrical 0.11 m-diameter with a 0.0095 m diameter shaft spinning at 170 RPM. The vessel height was set to 0.22 m, which, after accounting for the volume of the shaft, corresponds to a total gas volume of 1.721 L. The gas was assigned a density and viscosity of 1.225 kg/m^3 and 1.5 x 10^{-5} m^2/s. The gas inlet and outlet, which had diameters of 0.007 m and 0.015 m, are indicated in the figure. The inlet purge gas flow rate was 0.1 L/min, corresponding to a headspace turn over time of 1032 seconds. The outlet boundary was set to atmospheric pressure.

In Figure 6, we present a snapshot of the instantaneous velocity field across the headspace. A Taylor–Couette flow field is establish in the system, which is expected at this operating condition. (29) We observe that, following about 10 seconds operation, the flow field inside the vessel becomes steady. We also present a snapshot of the instantaneous gas concentration across the headspace fluid at various stages of the purge process. Released gas enters the headspace through a control volume positioned along the bottom 1 mm of the vessel. The time-evolution of the released gas flux into this control volume was defined by Equation 9 using the parameters presented in Figure 4. This control volume is designed to mimic the off-gassing effects of the slurry free surface. Throughout most of the purge, the release gas concentration is uniform throughout the vessel. In principle, the dynamic free surface will contribute to fluid motion. In practice, however, the velocity of the free surface is order-or-magnitude smaller than the velocity of the headspace gas near the interface. Note that, due to difference in density between the slurry and the headspace gas, bubble motion and release is not strongly coupled to the flow field/composition of the headspace.

For this two-gas system, the fluid viscosity is assumed to be constant. The local fluid density at each cell, however, is calculated using the local gas volume fraction:

$$\rho_{e,i} = \rho_h \phi_i + \rho_a (1 - \phi_i) \quad (11)$$

where $\rho_{e,i}$ and ϕ_i are the fluid density and released gas volume fraction lattice site i. The density of the released gas is set to 0.08 kg/m^3, consistent with the hydrogen generated in the experiment. The diffusion coefficient of the released gas was set to 7.5 x 10^{-5} m^2/s, a value typical of hydrogen in air. The snapshot presented here is characteristic of the complete off gassing process. Although the mean gas concentration decreases over time, the headspace remains well-mixed throughout the off-gassing process.

In Figure 7, we present the measured time-evolution of the released gas concentration at the nozzle exit. We superimpose on this measured data the predictions from the headspace model, as well as the analytical solution for two well-stirred tanks in series. This analytical solution is given by from:

$$C_H(t) = \frac{C_{s,o}}{(\tau_s/\tau_H - 1)} [\exp(-t/\tau_s) - \exp(-t/\tau_H)] \quad (12)$$

where $C_{s,o}$ and τ_s are initial concentration and release timescale of bubbles from the slurry, and τ_H is the headspace flow timescale defined from:

$$\tau_H = \frac{\dot{Q}_h}{V_h} \quad (13)$$

where $\dot{Q}_h$ is the gas flow rate through the headspace and V_h is the headspace volume. Note that Equation 12 is not valid for tanks with identical time constants (e.g. when $\tau_H = \tau_s$). The derivation of Equation 12 is presented in the Appendix.

The overall shape and trends predicted from the headspace simulation and Equation 12 are consistent with the measured headspace off-gassing data. Both approaches present an approximately 200 s time-shift relative to measured data, such that the models predict faster gas release than the measured data. There are several plausible causes for this time delay. One is the instantaneous release of the hydrogen gas when it reaches the slurry-gas interface. Adding additional physics to the model to account for the resistance to mass transfer across the interface would slow the release rate. Another is that the fluid in the model is single phase with a yield stress, while the fluid in the testing was a solid-liquid slurry. The presence of particles, surface active agents, and dissolved ions present in the material in the testing could provide another resistance to gas bubble release at the surface.

Most importantly, however, the experiment, simulation, and analytical solution each suggest that the characteristic timescale associated with variations in the headspace purge concentration are on the order of 1000 seconds. This value is much larger than ~100 s characteristic timescale associated with slurry off-gassing. This behavior has two important and related implications: (i) the overall response of the system is governed by the dynamics in the headspace and, by corollary, (ii) the time evolution of the purge gas concentration may not reflect the actual off-gassing rate of the slurry. In this case, the off-gassing occurs order-of-magnitude faster than might be inferred from head space measurements alone.

5.0 1 liter System

To further validate this approach, we repeat the procedure using measured off-gassing data obtained from a larger 1 L volume of slurry. From a modeling standpoint, we again decompose the system into (i) a slurry model used to predict the off-gassing rate and (ii) a headspace model used to predict the purge concentration. The slurry vessel, as illustrated in Figure 8, has a diameter of 0.11 m and a free surface level of 0.1 m. The slurry is agitated by two impellers, a Rushton and a pitch blade, both attached to the

same shaft and rotated at 300 RPM. Both impellers had a diameter of 0.051 m. The slurry was modeled as a yield stress fluid with the properties listed in Table 1.

The trapped gas bubbles were again modeled as 430,000 individual monodisperse spheres. Again, all bubbles were added to the tank instantaneously prior to the first simulation timestep and no additional bubbles were generated during agitation. The initial bubble size was set to 280 micrometers. Although more gas may be present, the volume fraction is low such that bubbles can be considered non-interacting. As such, although the number of modeled bubbles must be sufficient to characterize the off-gassing process, all bubbles do not need to be modeled explicitly.

In Figure 9, we present the time evolution of the bubble flux across the free surface interface for this 1 L system. Predictions in the model suggest a peak after about 40 seconds of agitation, followed by a gradual decrease in flux across the free surface. We again characterize the off-gassing by fitting this off-gassing data to Equation 9 using the initial gas volume of 4.91 mL The best fit value of τ_s is determined to be 621 seconds.

Again, deviations between the predicted off-gassing rate and expectations from the theoretical model in Equation 9 are indicative of non-ideal ideal mixing patterns within the fluid. In the first 100 seconds of agitation, for example, the fluid is accelerated by the impeller and converging to a steady state flow field. Accordingly, the predicted outgassing rates oscillate about expectations from Equation 9. After the start-up period, however, the predicted release rate follows first expectations from a well stirred system. As with the smaller system, this fit will be used as input to the headspace model, as well as input to the analytical solution.

In Figure 10, we present the headspace model used to simulate the headspace purge for this larger 1 L sample. The vessel was a cylindrical 0.10 m-diameter with a 0.005 m diameter shaft spinning at 300 RPM. The vessel height was set to 0.138 m, which, after accounting for the volume of the shaft, corresponds to a total gas volume of 1.080 L. The gas was assigned a density and viscosity of 1.225 kg/m^3 and 1.5 x 10^{-5} m^2/s. The gas inlet and outlet, which had diameters of 0.007 m and 0.015 m, are indicated in the figure. The inlet purge gas flow rate was 0.370 L/min, corresponding to a headspace turn over time of 172 seconds. The outlet boundary was set to atmospheric pressure. For this two-gas system, the fluid viscosity is assumed to be constant. The local fluid density at each cell, however, is calculated using Equation 11.

In Figure 11, we present the time-evolution of the cumulative released gas concentration at the nozzle exit. Unlike the instantaneous flux presented in Figure 7 for the 342 mL system, which is useful for characterizing the maximum off gassing rate, the cumulative data presented here is useful for characterizing the total off-gassing time. We superimpose on this measured data the predictions from the headspace model, as well as the analytical solution for two well-stirred tanks in series presented in Equation 12. The overall shape and trends predicted from the headspace simulation and Equation 12 are consistent with the measured headspace off-gassing data. Each approach suggests that, after approximately 1200 s, 80% of the trapped gas has been removed from the system.

In contrast to the 342 mL system, however, the measured headspace off-gassing of this 1 L vessel is more in line with the slurry off gassing rate. More specifically, in the 342 mL case, the off-gassing timescale was approximately 10x faster than head space purge timescale. Consequently, the measured response of the system is governed by headspace recirculation. For the 1 L system, however, the off-gassing timescale was approximately 4x *slower* than head space purge timescale. The measured

response of the system is therefore more closely linked to the slurry off-gassing. In practice, to minimize the need for time-scale deconvolution, the ratio of the off-gassing time scale to the head space purge timescale should be maximized. This behavior may also be important for operation, in order to minimize the concentration of hazardous gases in the headspace effluent. The agreement between the numerical simulation and the measured data at these two contrasting conditions, however, suggests that the model is mechanistically sound.

6.0 Full Scale System

We now apply this approach to understand off-gassing from a plant-scale 31.2 m^3 volume of slurry. From a modeling standpoint, we again decompose the system into (i) a slurry model used to predict the off-gassing rate and (ii) a headspace model used to predict the purge concentration. The slurry vessel, as illustrated in Figure 12, has a diameter of 3.66 m and a free surface level of 3.06 m. The plant scale tank also contains a cooling/heating coil assembly composed of three sets of 2-inch, Schedule 40 tubing. These coils, which have a pitch of 0.0914 m and are concentrically oriented about the center of the tank, have diameters of 1.18, 1.33, and 1.5 m. The slurry is agitated by two impellers: a four-blade radial flow impeller near the bottom of the cooling coil assembly, and a three-blade axial downward flow impeller near the top of the cooling coil assembly. Both impellers had a diameter of 0.91 m and were rotated at 130 RPM. The slurry was modeled as a yield stress fluid with the properties listed in Table 1. The trapped gas bubbles were again modeled as 100,000 individual 310 micrometer spheres. Again, all bubbles were added to the slurry uniformly and instantaneously prior to the first simulation timestep.

In Figure 13, we present the time evolution of the bubble flux across the free surface interface for this 31.2 m^3 system. Predictions in the model suggest a peak after about 208 seconds of agitation, followed by a gradual decrease in flux across the free surface. We again characterize the off-gassing by fitting this

off-gassing data to Equation 9 using the initial gas volume of 1.6 mL. The best fit value of τ_s is determined to be 2273 seconds.

In Figure 14, we present the headspace model used to simulate the headspace purge for the 31.2 m^3 system. The vessel was a cylindrical 3.66 m-diameter with a 0.1 m diameter shaft spinning at 130 RPM. The vessel height was set to 0.96 m, which, after accounting for the volume of the shaft, corresponds to a total gas volume of 10.33 m^3. The gas was assigned a density and viscosity of 1.225 kg/m^3 and 1.5 x 10^{-5} m^2/s. The gas inlet and outlet, which had diameters of 0.34 m and 0.5 m, are indicated in the figure. The inlet purge gas flow rate was 7702 L/min, corresponding to a headspace turn over time of 85 seconds.

In Figure 15, we present the predicted time-evolution of the cumulative released gas concentration at the nozzle exit. We superimpose on this predicted data the analytical solution for two well-stirred tanks in series presented in Equation 12. The overall shape and trends predicted from the headspace simulation and Equation 12 are consistent: each approach suggests that, after approximately 2000 s, 80% of the trapped gas has been removed from the system. Measured off-gassing data, as presented for the 342 mL and 1 L scale systems, is not available for the full-scale systems. The predicted release timescales and gas concentrations, however, are in-line with operator reports.

7.0 Guidance on Operating Conditions

The slurry off-gassing results presented here are specific to the operating conditions at each scale and the fluid properties listed in Table 1. To help generalize these findings to other systems, we examined the sensitivity of the slurry off-gassing time scales to the slurry properties, bubble properties, and impeller speed. Many properties had little effect on the gas release rate. Varying the bubble diameter

between 10 and 310 micrometers, for example, presented no material change in the off-gassing rate. This behavior is expected, given the small size and Stokes numbers of the bubbles. Likewise, for systems with bubble volume fractions below 0.1%, the off-gassing rate was largely insensitive to bubble number. The release rate was also largely insensitive to 5-10% variations in slurry density. This result is not surprising, since the slurry density is already three orders-of-magnitude larger than the gas bubble density.

Two system properties that strongly influence the off-gassing rate are (i) the impeller speed and (ii) the fluid yield stress. This behavior is expected, as these parameters compete to inform the cavern diameter within the fluid. More specifically, the cavern diameter D_c is expected to be a function of the impeller tip speed and yield stress via:

$$\left(\frac{D_c}{D}\right)^3 = 1.36\left(\frac{N_p}{\pi^2}\right)\frac{V_t^2}{\sigma} \quad (14)$$

where N_p is the impeller power number, V_t is the impeller tip speed, and σ is the specific yield stress. (27) In the 342-ml system, for example, the set impeller speed of 170 RPM generates a cavern equal to the tank diameter. This principle was understood during process development and motivated the selected impeller speed. If the impeller speed in the simulation is decreased to 150 RPM, the cavern no longer reaches the tank wall and the predicted slurry off-gassing timescale increases by an order-of-magnitude.

This behavior is further corroborated by simulations of the fully-scale system. At the set impeller speed of 130 RPM, Equation 14 suggests that the full-scale tank will remain fully agitated for slurries with a yield stress up to 50 Pa. In the simulation, increasing the slurry yield stress from the base-line value of 7.2 Pa to elevated values of 10 Pa and 20 Pa has no strong effect on the predicted off-gassing timescale.

Increasing the yield stress above this critical value of 50 Pa, however, induces longer gas releases times due to reduced cavern formation.

8.0 **Conclusion**

We have presented first principles modeling approaches for predicting gas release from agitated two-phase slurries and gas transport within an attached purged headspace. This slurry approach uses the physical properties of the fluids and the topology of the system to directly predict the gas release rate. The headspace model uses the off-gassing rate from the slurry, as well as the headspace geometry and purge rates to predict the time evolution of the headspace concentration. Although the slurry model presents explicit insights into the gas release rate, the headspace model makes predictions that are more immediately comparable to measured data.

Predictions from the model agree well with measured off-gassing data at two different scales and operating conditions. The predictions also were consistent with an exact solution for two well-stirred systems in series. In fact, if the slurry or headspace are well stirred, a physics based numerical model is not necessary and the response of the system can be predicted analytically. This numerical approach can also help to deconvolute measured purge gas data, using the mean residence time of the headspace. It can also be used to understand the sensitivity of the off-gassing rate to fluid properties and agitation conditions.

Appendix

The time-evolution of the trapped gas concentration in the headspace C_2 can be predicted from the conservation of mass. For a well stirred system, this expression becomes:

$$\frac{dC_H}{dt} = [C_o/\tau_s] \exp\left(-\frac{t}{\tau_s}\right) - C_H/\tau_H \quad \text{(A-1)}$$

where V_h is the volume of the headspace, C_o is the initial volume of gas in the slurry, τ_s is the slurry off-gassing time scale, and τ_H is the headspace turnover time scale given by:

$$\tau_H = \frac{\dot{Q}_h}{V_h} \quad \text{(A-2)}$$

where $\dot{Q}_h$ is the gas flow rate through the headspace. The first term on the right-hand side of Equation (A-1) describes mass flux into the headspace from the slurry. The second term is the mass flux leaving the headspace outlet. Equation (A-1) is a linear, first order differential equation with variable coefficients. This equation can be solved using the method of integrating factors. If the headspace is initially free of released gas, such that $C_{2,o} = 0$, and $\tau_2 \neq \tau_1$, Equation (A-1) has the exact solution presented given by:

$$C_H(t) = \frac{C_{s,o}}{(\tau_s/\tau_H - 1)} [\exp(-t/\tau_s) - \exp(-t/\tau_H)] \quad \text{(A-3)}$$

Recognize that this solution is only valid for $\tau_H \neq \tau_S$.

References

1. *Yield Stress Dependency on the Evolution of Bubble Populations Generated in Consolidated Soft Sediments.* **M. Johnson, M. Fairweather, D. Harbottle, T. N. Hunter, J. Peakall, and S. Biggs.** 9, 2017, AIChE J, Vol. 63, pp. 3728-3742.

2. *Hydrogen Generation Rates in Savannah River Site High-Level Nuclear Waste.* **D. T. Hobbs, P. W. Norris, S. A. Pucko, N. E. Bibler, D. D. Walker, and P. D. d'Entremont.** Tucson, AZ : s.n. Proceedings Waste Management '92 Meeting.

3. *Motion and Shape of Bubbles Rising through a Yield Stress Fluid.* **Sikorski D., Tabuteau H., and de Bruyn, J. R.** 2009, J Non-Newtonian Fluid Mech, Vol. 159, pp. 10-16.

4. *Steady bubble rise and deformation in Newtonian and viscoplastic fluids and conditions for bubble entrapment.* **Tsamopoulos, J., Dimakopoulos, Y., Chatzidai, N., Karapetsas, G., & Pavlidis, M. (). . , 601,.** s.l. : Journal of Fluid Mechanics, 2008, Vol. 601, pp. 123-164.

5. **Rassat S.D., Gauglitz P.A., Bredt P.R., Mahoney L.A., Forbes S.V., and Tingey S.M.** *Mechanisms of gas retention and release: Experimental Results for Hanford Waste Tanks 241-AW-101 and 241-AN-103.* Richland, WA (United States) : Pacific Northwest Lab, 1997. PNNL-11642.

6. **Gauglitz, P. A., S. D. Rassat, and M. R. Powell.** *Gas bubble retention and its effect on waste properties: Retention mechanisms, viscosity, and tensile and shear strengths.* Richland, WA (United States) : Pacific Northwest Lab, 1995. PNL-10740..

7. **Russell, S.D. et al.** *Final Report Gas Retention and Release in Hybrid Pulse Jet Mixed Tanks Containing non-Newtonian Waste Simulants.* Richland, Washington : Battelle--Pacific Northwest Division, 2005. PNWD-3552.

8. *Gas Retaining and Release Experiments with Low Yield Stress Fluids.* **Patel R., Tachiev, G., Yadaz N., Awwad, A. , McDaniel, D. , and Roelant, D.** Phoenix, AZ. : Waste Management , 2011. 11289.

9. *Implementation of proton transfer reaction-mass spectrometry (PTR-MS) for advanced bioprocess monitoring.* **Luchner, M., Gutmann, R., Bayer, K., Dunkl, J., Hansel, A., Herbig, J., Singer, W., Strobl, F., Winkler, K. and Striedner, G.** 12, s.l. : Biotechnology and bioengineering, 2012, Vol. 109, pp. 3059-3069.

10. *Mini-review: Soft sensors as means for PAT in the manufacture of bio-therapeutics.* **Mandenius, Carl-Fredrik, and Robert Gustavsson.** 2, s.l. : Journal of Chemical Technology & Biotechnology, 2015, Vol. 90, pp. 215-227.

11. *Motion and Shape of Bubbles Rising through a Yield Stress Fluid.* **D. Sikorski, H. Tabuteau, and J. R. de Bruyn.** s.l. : J Non-Newtonian Fluid Mech, 2009, Vol. 159, pp. 10-16.

12. *Steady Bubble Rise and Deformation in Newtonian and Viscoplastic Fluids and Conditions for Bubble Entrapment.* **J. Tsamopoulos, Y. Dimakopoulos, N. Chatzidal, G. Karapetsas, and M. Pavlidis.** s.l. : J Fluid Mech, 2008, Vol. 601, pp. 123-164.

13. **C. O. Bennett and J. E. Myers, Momentum.** Heat, and Mass Transfer. 3. New York : McGraw-Hill, 1982.

14. **Succi, Sauro.** *The lattice Boltzmann equation: for fluid dynamics and beyond.* s.l. : Oxford University Press, 2001.

15. **Krüger, T., Kusumaatmaja, H., Kuzmin, A., Shardt, O., Silva, G., Viggen, E.M.** *The Lattice Boltzmann Method.* s.l. : Springer International Publishing, 2017.

16. *An immersed boundary method based on the lattice Boltzmann approach in three dimensions, with application.* **Zhu, Luoding, Guowei He, Shizhao Wang, Laura Miller, Xing Zhang, Qian You, and Shiaofen Fang.** 12, 2011, Computers & Mathematics with Applications, Vol. 61, pp. 3506-3518.

17. *A conservative phase field method for solving incompressible two-phase flows.* **Lin, Pao-Hsiung Chiu and Yan-Ting.** 1, 2011, Journal of Computational Physics, Vol. 230, pp. 185-204.

18. *A coupled lattice Boltzmann method and discrete element method for discrete particle simulations of particulate flows.* **Rüde., Christoph Rettinger and Ulrich.** 2018, Computers & Fluids , Vol. 172, pp. 706-719.

19. *Sphere Drag and Settling Velocity Revisited.* **Brown, P.P. and Lawler, D.F.** 129, s.l. : J. Environ. Chem. Eng., 2003, pp. 222-231.

20. **Tildesley., Michael P Allen and Dominic J.** *Computer simulation of liquids.* 2nd. s.l. : Oxford University Press, 2017.

21. ***M-Star CFD.*** *2020.*

22. ***Shu, Zhaoli Guo and Chang.*** *Lattice Boltzmann method and its applications in engineering. s.l. : World Scientific, 2013.*

23. Towards overcoming the LES crisis. ***Löhner, Rainald.*** *3, 2019, International Journal of Computational Fluid Dynamics, Vol. 33, pp. 87-97.*

24. A CFD Digital Twin to Understand Miscible Fluid Blending. ***John Thomas, Kushal Sinha, Gayathri Shivkumar, Lei Cao, Marina Funck, Sherwin Shang and Nandkishor Nere.*** *2021, AAPS PharmSciTech, p. 91.*

25. A mechanistic approach for predicting mass transfer in bioreactors. ***John A. Thomas, Xiaoming Liu, Brian DeVincentis, Helen Hua, Grace Yao, Michael C. Borys, Kathryn Aron, Girish Pendse.*** *2021, Chemical Engineering Science, p. 116538.*

26. Bubble Sizes in Electrolyte and Alcohol Solutions in a Turbulent Stirred Vessel. ***Machon, V., Pacek, A.W. and Nienow, A.W.*** *s.l. : Chem. Eng. Res. Des., 1997, Vol. 75, pp. 339–348.*

27. ***Paul, Edward L., Atiemo-Obeng, Victor A., Kresta, Suzanne M. (Eds.),.*** *Handbook of Industrial Mixing: Science and Practice. s.l. : John Wiley & Sons, 2004.*

28. ***Doran, Pauline M.*** *Bioprocess Engineering Principles 2nd Edition. s.l. : Academic Press, 2012.*

29. ***White, Frank.*** *Fluid Mechanics, 5th Edition. New York : McGraw Hill, 2003. pp. 25–36. Vol. 76.*

Table 1: Slurry rheology for lab-scale and pilot scale tests and full-scale vessel

Slurry Property	342 ml System	1 L System	32.2 m^3 System
Density, ρ (kg/m^3)	1270	1140	1160
Yield Stress, τ_o (Pa)	4.06	6.80	7.2
Consistency Index, k, (Pa-s)	0.0074	0.0086	0.0091
Flow index, n, (-)	1.0	1.0	1.0

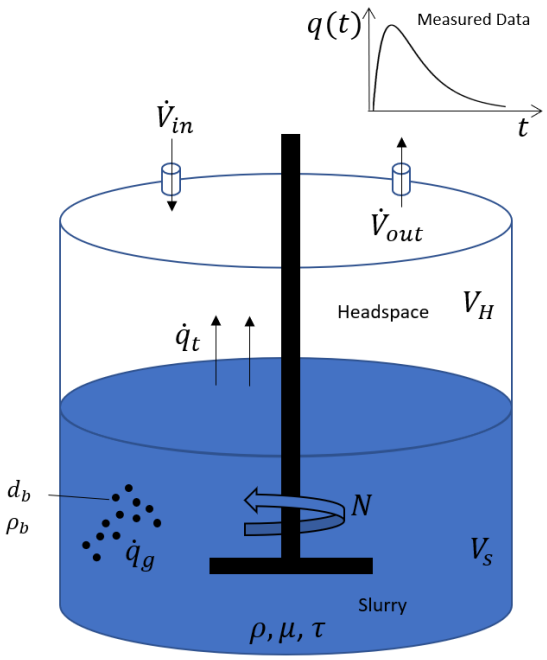

Figure 1: The relevant parameters governing off-gassing and head space characterization.

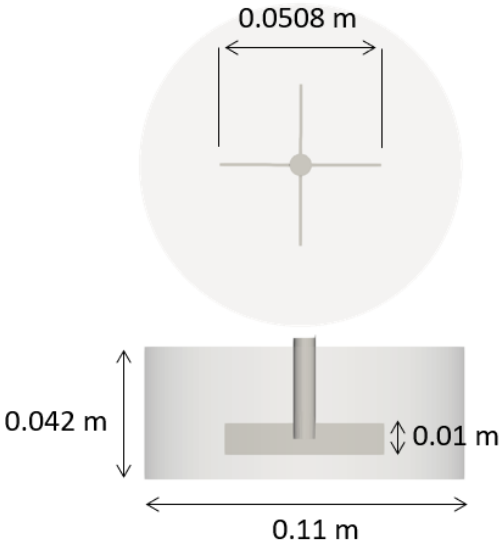

Figure 2: Geometry of 342 mL slurry simulation. The agitator is a flat blade impeller.

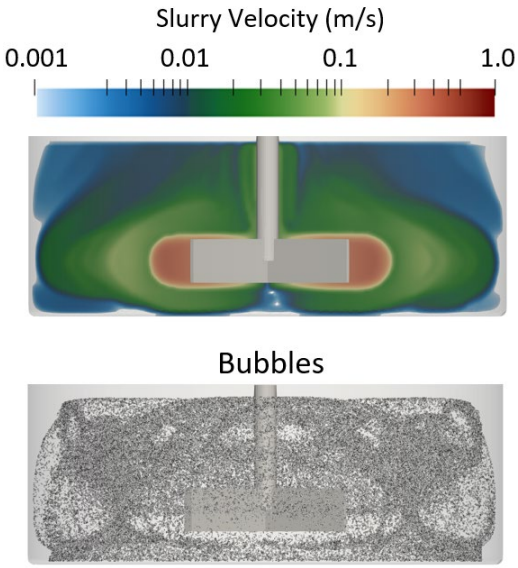

Figure 3: (Top) Instantaneous slurry velocity along a plane cut through the center of the vessel after 10 seconds of agitation. The color scale maps logarithmically to color, highlighting high velocity near the impeller relative to that near the walls. Although most of the fluid is agitated fluid dead zones persist near the walls and in the corners of the vessel. (Bottom) Snapshot of the bubble field after 10 seconds of agitation. Although the bubbles follow the velocity striations, they remain well distributed across the fluid through the release process.

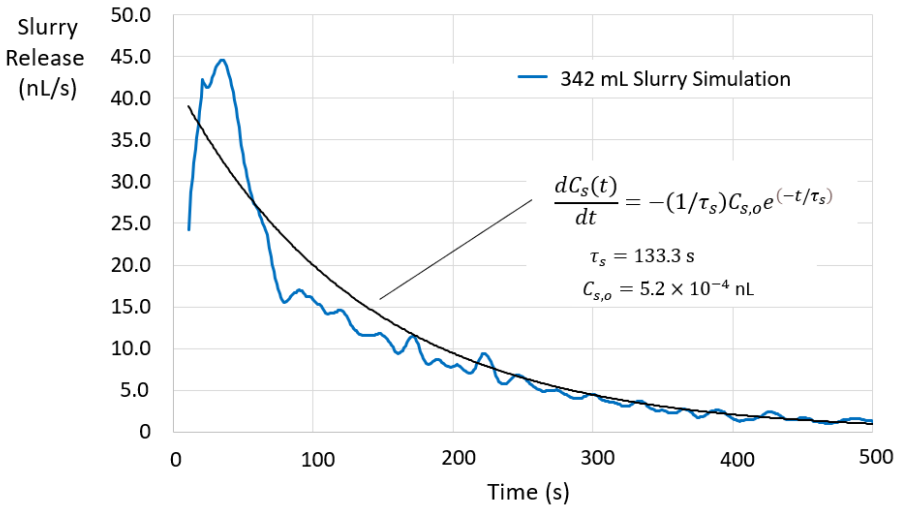

Figure 4: Predicted slurry gas release rate over time for the 342 mL system. Superimpose on this predicted data is a best-fit parameterization of Equation 8. The initial gas concentration is known. The predicted release time scale, $\boldsymbol{\tau_s}$, is tuned to optimized the fit.

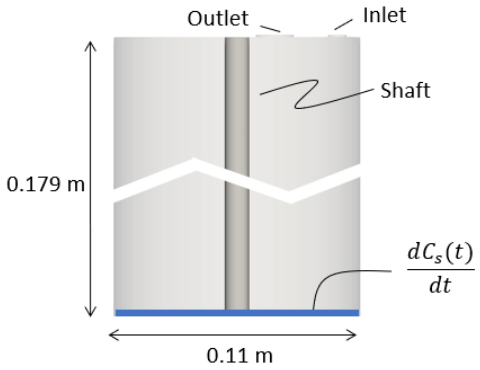

Figure 5: Headspace geometry for the 342 mL slurry system.

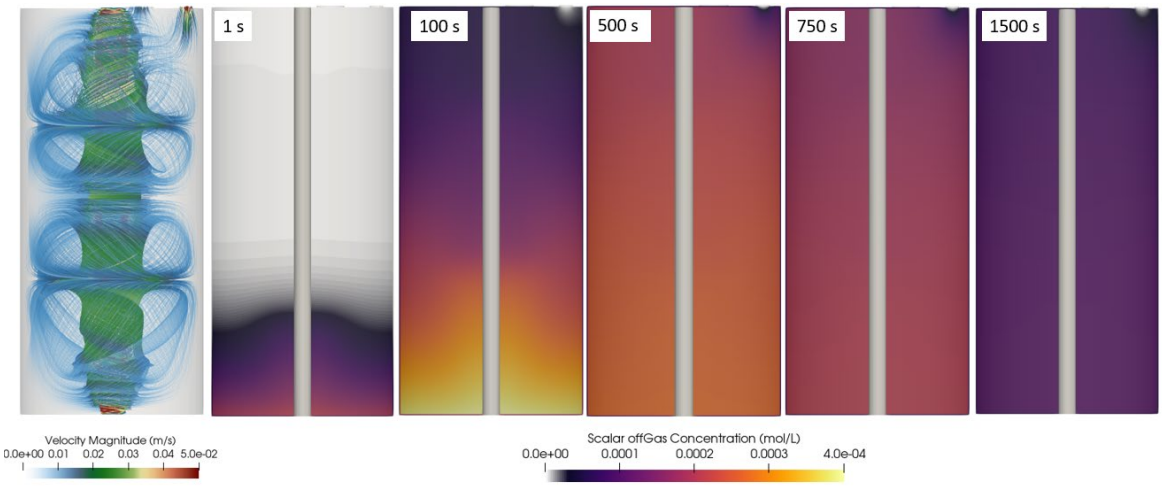

Figure 6: (Left) Streamlines of the instantaneous gas velocity in the headspace after 100 seconds of simulation. The motion of the impeller shaft introduces a Taylor–Couette flow field within the vessel. (Right) Snapshots of the instantaneous concentration of the released gas. Following the initial slurry off gassing, the released gas (hydrogen in this case) is well stirred throughout the off-gassing process.

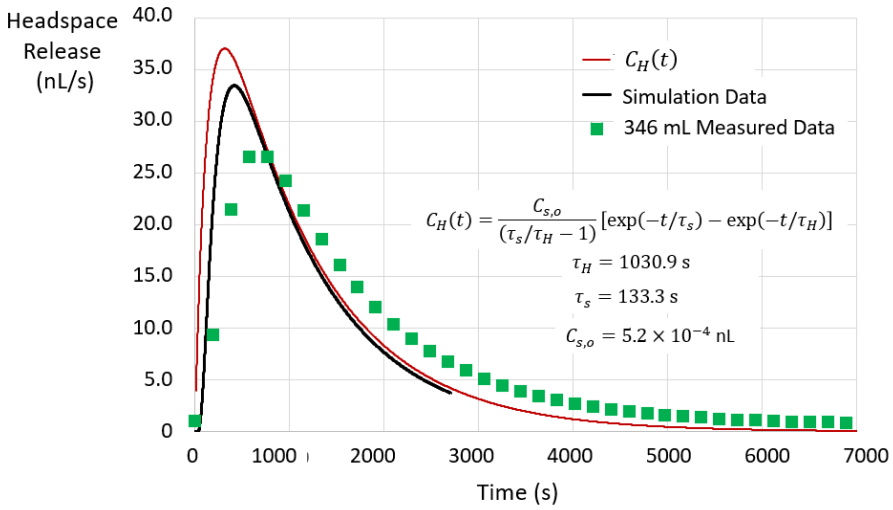

Figure 7: Measured, simulation, and calculated time-evolution of the head space gas release. Each approach predicts a release time on the order of 1000 seconds. This time scale is much longer that the slurry off-gassing time scale, which is on the order of 100 s.

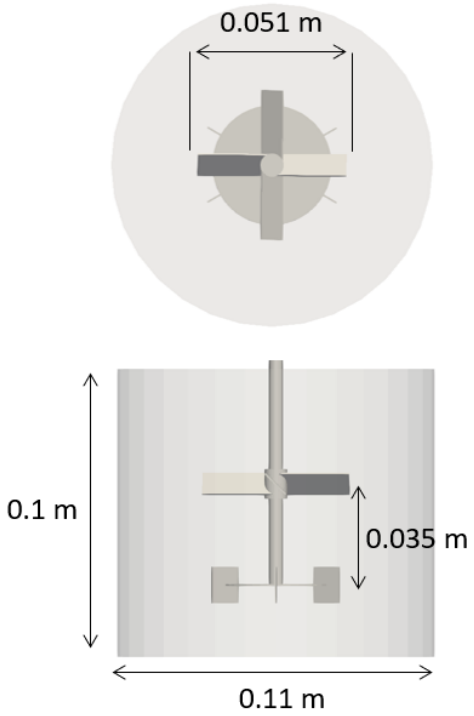

Figure 8: Geometry of 1 liter slurry simulation. The tank is agitated by a Rushton and pitch blade impeller.

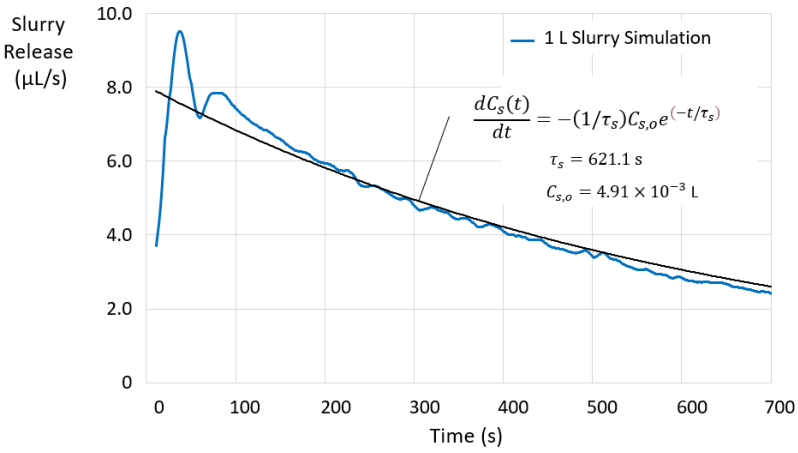

Figure 9: Predicted slurry gas release rate over time for the 1L system. Superimposed on this predicted data is a best-fit parameterization of Equation 8. The initial gas concentration is known. The predicted release time scale, $\boldsymbol{\tau_s}$, is tuned to optimize the fit.

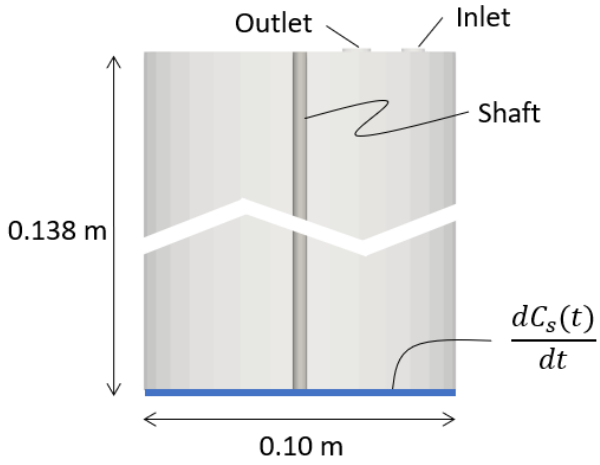

Figure 10: Headspace geometry for the 1 liter slurry system.

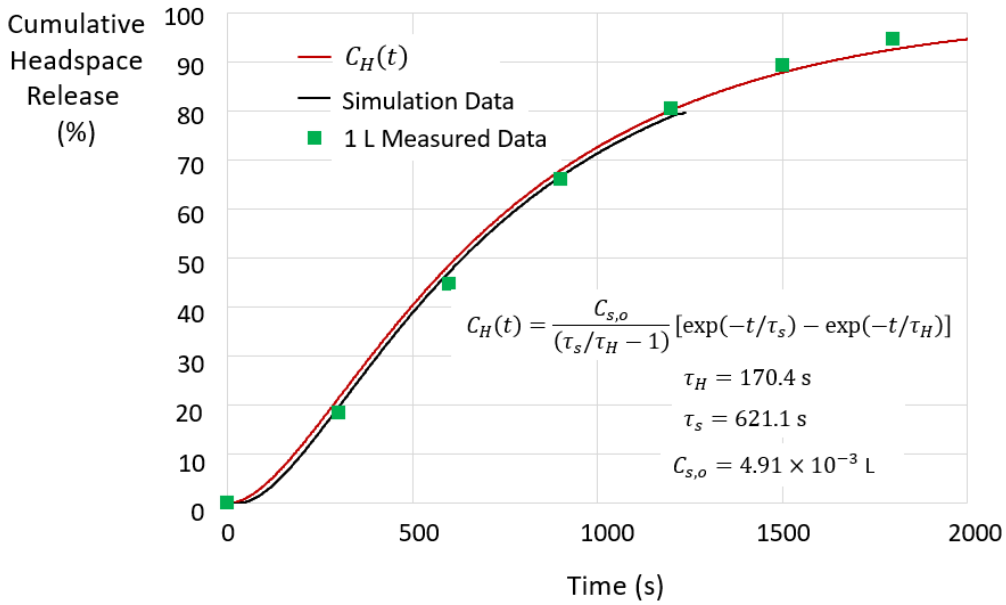

Figure 11: Simulated, calculated, and measured time-evolution of cumulative head space gas release. Each approach predicts a release time on the order of 1000 seconds.

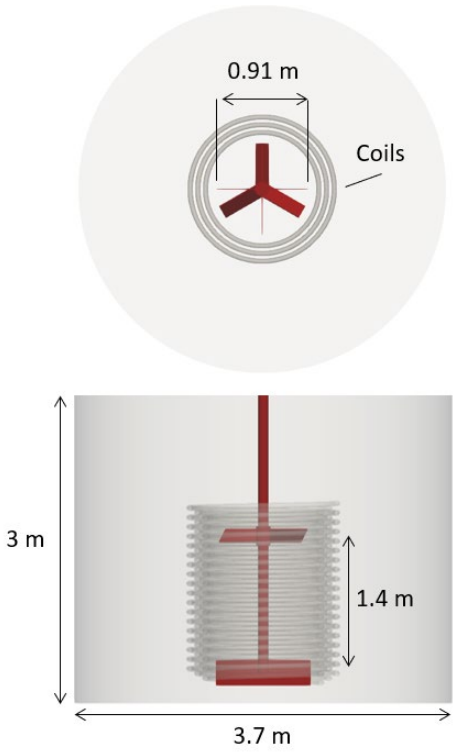

Figure 12: Geometry of 32.2 m^3 slurry simulation. The tank is agitated by a flat blade and pitch blade impeller. Three sets of concentric heating/cooling coils surround the impeller.

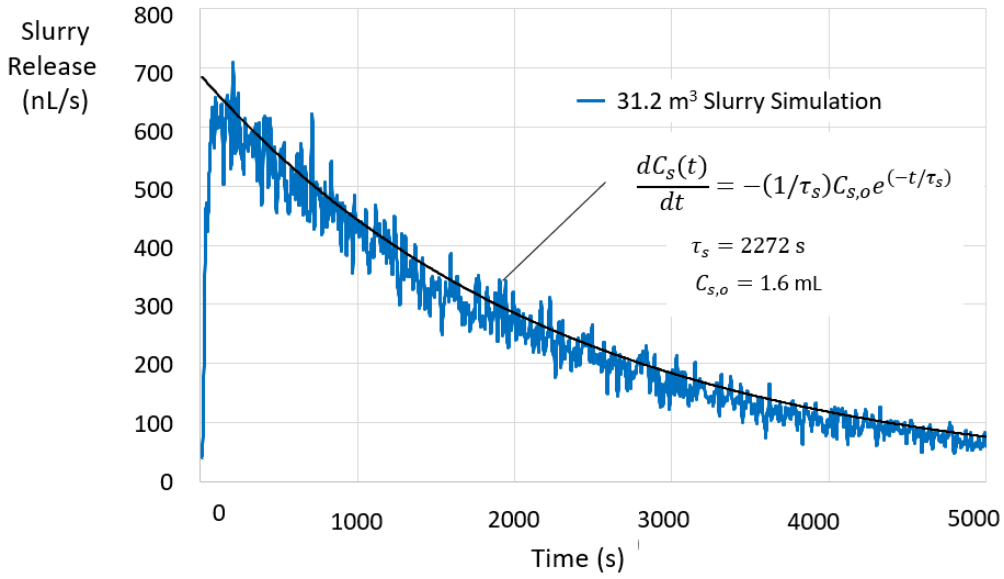

Figure 13: Release of Hydrogen from Slurry in the Full-Scale Vessel

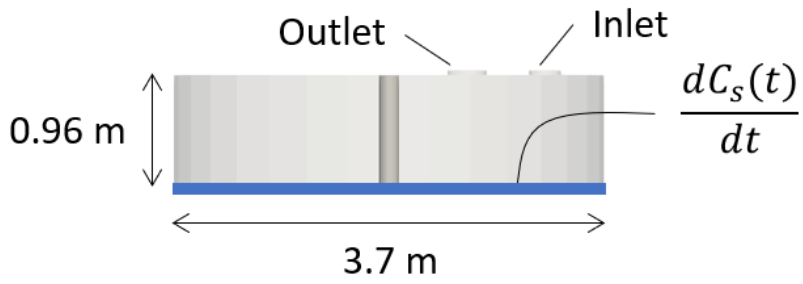

Figure 14: Headspace geometry of 31.2 m^3 slurry system

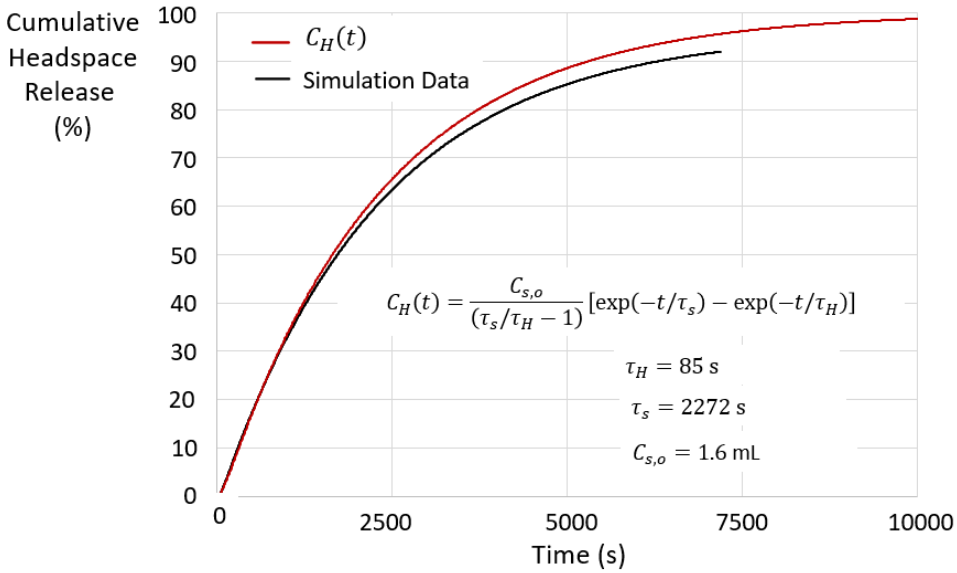

Figure 15: Simulated and calculated time-evolution of cumulative head space gas release. Each approach predicts a release time on the order of 3000 seconds.

Acknowledgements

This work was produced by Battelle Savannah River Alliance, LLC under Contract No. 89303321CEM000080 with the U.S. Department of Energy. Publisher acknowledges the U.S. Government license to provide public access under the DOE Public Access Plan (http://energy.gov/downloads/doe-public-access-plan).

Note:

The paper was submitted to Chemical Engineering Science for publication